J. Fluid Mech. (2006), *vol.* 563, *pp.* 261–281.
doi:10.1017/S0022112006001273 Printed in the United Kingdom

Low-frequency spectra in a harbour excited by short and random incident waves

By MENG-YI CHEN[1], CHIANG C. MEI[1] AND CHIEN-KEE CHANG[2]

[1]Department of Civil and Environmental Engineering, Massachusetts Institute of Technology, Cambridge, MA 02139, USA

[2]Harbour Research Institute, Taichung, Taiwan

(Received 17 November 2005 and in revised form 21 February 2006)

We present a spectral theory of the low-frequency response of a harbour to short and random incident waves. Assuming the incident sea to be stationary and Gaussian, nonlinear extensions are made for the response spectrum. Advantage is taken of the typical wind-wave spectrum which is dominated by high-frequency components. After showing that nonlinearity is needed only up to the second order in wave steepness, we extend the mild-slope approximation for constructing the transfer functions. Numerical examples are presented for a square harbour and constant depth. Discounting friction losses, the effects of different entrances are compared.

1. Introduction

Harbours are designed to shelter ships from storm-induced sea waves. Long-period oscillations with periods of one to several minutes often occur, however, inside harbours which can cause excessive sway of ships, resulting in damage to ship hulls or mooring systems, or costly delay of loading and unloading operations. The most studied mechanism is the synchronous resonance by tsunamis which are themselves of very long periods (10 minutes to an hour). In this case the linear theory of wave scattering, well-known in physics, has been extended both analytically and numerically (Miles & Munk 1961; Lee & Raichlan 1972; Hwang & Tuck 1970; Chen & Mei 1974, etc.; review can be found in Mei 1983 or Mei Stiassnie & Yue 2005). However, many harbours in the world are attacked much more often by the short incident waves generated by storms, rather than by tsunamis. Field records from Hualien Harbour on the eastern (Pacific) coast of Taiwan are typical. Figure 1(*c*) shows the wave records at several stations marked in the figure 1(*b*), during Typhoon Tim, 1994. It is clear that oscillations measured at Stations 8 and 10 inside the basin are dominated by low frequencies, unlike the records at Station 2 outside. During Typhoon Longwang on October 2, 2005, a 7000-ton cargo ship, originally moored near the northern end of the basin, broke loose and drifted for 1 km southward, then ran aground outside the harbour and broke up.

In the engineering practice of harbour design and renovation, the linear mechanism is still widely used as the basis of both theoretical and experimental modelling, by hypothesizing or estimating the intensity of an incident wave with periods that are of concern in the harbour. As long waves are known to occur by nonlinearity due to quadratic mixing of short waves of nearly equal frequencies, improved theories for narrow-banded and deterministic waves have been proposed by Bowers (1977),

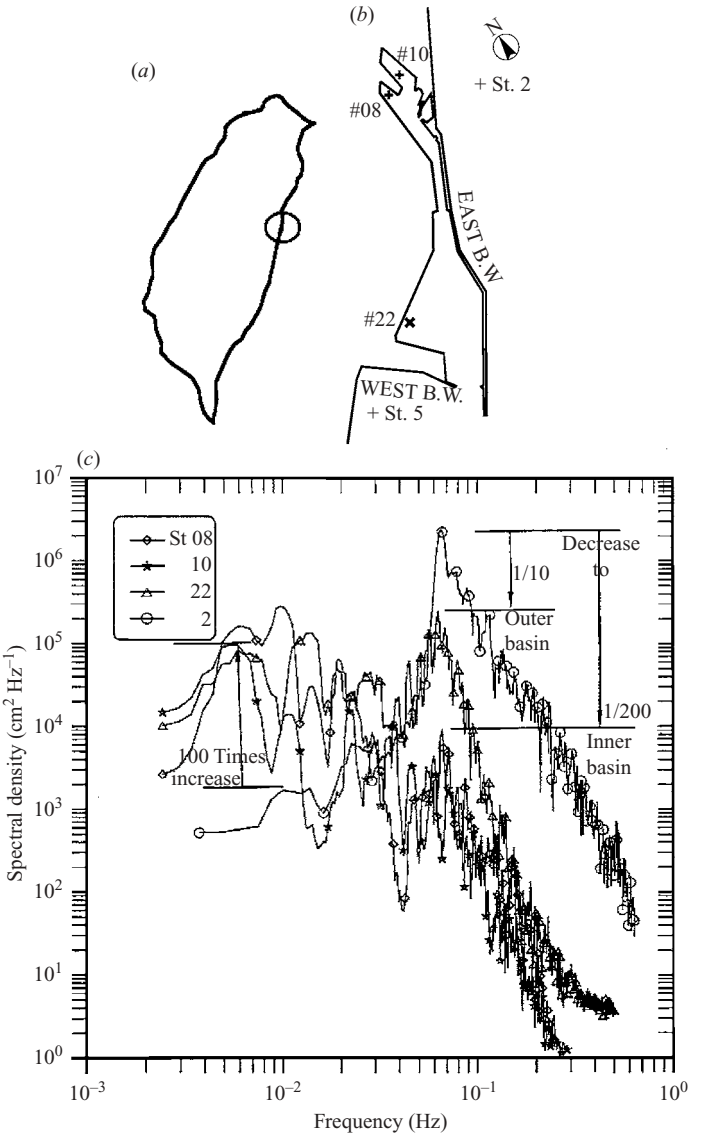

FIGURE 1. (*a*) Taiwan Island. Circle indicates Hualien Harbour facing the Pacific Ocean. (*b*) Plan of Hualien Harbour with sites of wave-recording stations. Measuring Stations 8 and 10 are at the northern corner of the basin. Stations 2 and 5 are outside. (*c*) Wave spectra at various stations recorded during Typhoon Tim, 1994. Record for Station 5 is omitted.

Mei & Agnon (1989), Wu & Liu (1990). These theories are however inadequate for representing wind-induced waves which are random and broad-banded.

Vital to wave forecasting, modelling of nonlinear progressive waves in the open sea is a highly developed, and still developing, branch of oceanography (Koman *et al.* 1994). Of greater relevance to coastal engineering however, are the effects of complex coastlines and bathymetry. A theory of long-wave excitation by short waves must in general account not only for randomness and nonlinearity, but also for diffraction and refraction. For two-dimensional standing waves in deep water, Sclavounos (1992) has advanced a systematic stochastic theory for calculating the nonlinear corrections

of the spectrum. By assuming the incident waves to be a stationary and Gaussian random process, he showed that the correction starts at the fourth order in wave steepness, and depends on the frequency responses at first, second and third orders. With emphasis on the small corrections for the entire frequency range, he presented numerical results from the explicit solutions of the frequency responses which are two-dimensional and relative simple to derive.

For the prediction of low-frequency spectra in harbours, in this article we generalize the spectral theory of Sclavounos, and, for calculating the nonlinear transfer function, the second-order mild-slope approximation developed recently for monochromatic incident waves (Chen & Mei 2006). This approximation reduces the three-dimensional diffraction problems at both orders to two dimensions. Thanks to the coincidence of two special features, one in the stochastic theory, and the other in the common characteristics of the coastal sea, only the second-order frequency response suffices. While the general theory can account for both lateral geometry and bathymetry, numerical examples are given only for constant depth and a simple planform in order to focus attention on the physical consequence of sheltering. Effects of the harbour entrance are examined.

2. Formulation of nonlinear problem

For convenience we first summarize the perturbation equations for small-amplitude waves, based on the usual assumptions of an incompressible and inviscid fluid, and irrotational flow. Expand in powers of the wave steepness $\epsilon = O(kA)$:

$$\Phi = \Phi_1 + \Phi_2 + \cdots, \quad \zeta = \zeta_1 + \zeta_2 + \cdots, \tag{2.1}$$

where k is the characteristic wavenumber, A is the characteristic amplitude. The subscripts indicate the order of magnitude in powers of ϵ, i.e. $\Phi_1 = O(\epsilon)$, $\Phi_2 = O(\epsilon^2)$, etc. Let the horizontal and three-dimensional gradient operators be distinguished by ∇_2 and ∇_3. At each order, Φ_j satisfies the Laplace equation

$$\left(\nabla_2^2 + \frac{\partial^2}{\partial z^2}\right)\Phi_j = 0, \quad j = 1, 2, 3, \ldots \tag{2.2}$$

in the fluid, and

$$\frac{\partial \Phi_j}{\partial z} = \nabla_2 h \cdot \nabla_2 \Phi_j, \quad z = -h(x, y), \qquad j = 1, 2, 3, \ldots \tag{2.3}$$

on the sloping seabed. All lateral boundaries are assumed for simplicity to be vertical throughout the depth, hence

$$\frac{\partial \Phi_j}{\partial n} = 0, \qquad j = 1, 2, 3, \ldots \tag{2.4}$$

where $\boldsymbol{n}$ is in the horizontal plane. On the still water surface, $z = 0$, the boundary condition for the first-order potential is homogeneous:

$$g\frac{\partial \Phi_1}{\partial z} + \frac{\partial^2 \Phi_1}{\partial t^2} = 0, \quad z = 0, \tag{2.5}$$

while that for the second-order potential is not:

$$\frac{\partial \Phi_2}{\partial z} + \frac{1}{g}\frac{\partial^2 \Phi_2}{\partial t^2} = \frac{1}{g^2}\frac{\partial \Phi_1}{\partial t}\frac{\partial}{\partial z}\left[g\left(\frac{\partial \Phi_1}{\partial z}\right) + \frac{\partial^2 \Phi_1}{\partial t^2}\right] - \frac{1}{g}\frac{\partial}{\partial t}\left(\nabla_3 \Phi_1\right)^2, \quad z = 0. \tag{2.6}$$

The free-surface displacement at the first order, ζ_1, is related to Φ_1 by

$$\zeta_1 = -\frac{1}{g}\left[\frac{\partial \Phi_1}{\partial t}\right]_{z=0}. \tag{2.7}$$

The second-order correction, ζ_2, is the sum of two parts,

$$\zeta_2 = \zeta_2^{(1)} + \zeta_2^{(2)}, \tag{2.8}$$

where

$$\zeta_2^{(1)} = \left[\frac{1}{g^2}\frac{\partial \Phi_1}{\partial t}\frac{\partial^2 \Phi_1}{\partial t \partial z} - \frac{1}{2g}(\nabla_3 \Phi_1)^2\right]_{z=0}, \tag{2.9}$$

and

$$\zeta_2^{(2)} = \left[-\frac{1}{g}\frac{\partial \Phi_2}{\partial t}\right]_{z=0}. \tag{2.10}$$

The first part $\zeta_2^{(1)}$ can be immediately calculated from the first-order solution, while the second $\zeta_2^{(2)}$ depends on the second-order potential Φ_2 which is the task here.

3. Correlation and frequency spectrum

We now extend the stochastic approach of Sclavounos (1992) from two-dimensional standing waves in deep water to scattering by a more complex bathymetry and coastline geometry. A basic assumption is that the free-surface height is a stationary and Gaussian random process. Denoting ensemble averages by overlines, we define the correlation function of the total free-surface height $\zeta(x, y, t)$ by

$$H(x, y, \tau) = \overline{\zeta(x, y, t)\,\zeta^*(x, y, t+\tau)} \tag{3.1}$$

where ζ^* denotes the complex conjugate of ζ. (Since ζ is real it is equal to ζ^*. The choice in the definition (3.1) facilitates the treatment of Fourier transforms.) The corresponding frequency spectrum S is its Fourier transform,

$$S(x, y, \omega) = \frac{1}{2\pi}\int_{-\infty}^{\infty} \mathrm{d}\tau\, \mathrm{e}^{\mathrm{i}\omega\tau} H(x, y, \tau). \tag{3.2}$$

Introducing the expansion (2.1), the total correlation function of the free surface comprises quadratic products (ζ_1, ζ_1) at order $O(\epsilon^2)$, (ζ_1, ζ_2) at $O(\epsilon^3)$, and (ζ_2, ζ_2) and (ζ_1, ζ_3) at $O(\epsilon^4)$. Since $\zeta_1, \zeta_2, \zeta_3, \ldots$ involve Fourier transforms with integrands proportional to $A, AA, AAA, \ldots$ respectively, the right-hand side of (3.1) involves ensemble averages of even and odd products of A. Due to Gaussianity, all odd products give zero averages, while all even products can be reduced to averages of quadratic products. It follows that nonlinear corrections begin at $O(\epsilon^4)$,

$$H(\tau) = H_2(\tau) + H_4(\tau) + \cdots \tag{3.3}$$

where the dependence on (x, y) is not shown for the sake of brevity and

$$H_2(\tau) = \overline{\zeta_1(t)\,\zeta_1^*(t+\tau)} \quad \text{and} \quad H_4(\tau) = H_{22}(\tau) + H_{13}(\tau) + H_{31}(\tau) \tag{3.4}$$

are of $O(\epsilon^2)$ and $O(\epsilon^4)$ respectively with

$$H_{22} = \overline{\zeta_2(t)\,\zeta_2^*(t+\tau)}, \quad H_{13} = \overline{\zeta_1(t)\,\zeta_3^*(t+\tau)}, \quad H_{31} = \overline{\zeta_3(t)\,\zeta_1^*(t+\tau)}. \tag{3.5}$$

The corresponding frequency spectrum is

$$S(\omega) = S_2(\omega) + S_4(\omega) + \cdots \tag{3.6}$$

where S_2 is the Fourier transform of H_2 as defined by (3.2). The nonlinear correction is

$$S_4(\omega) = S_{22}(\omega) + S_{13}(\omega) + S_{31}(\omega) \tag{3.7}$$

where S_{22}, S_{13} and S_{13} are respectively the Fourier transforms of H_{22}, H_{13} and H_{31}.

For convenience and clarity, we first recall the statistical description of the leading-order waves. Let the free-surface displacement be

$$\zeta_1^{(I)}(x, y, t) = \int_{-\infty}^{\infty} A(\omega)\, \mathrm{e}^{\mathrm{i}\boldsymbol{k}\cdot\boldsymbol{x}-\omega t}\, \mathrm{d}\omega = \int_{-\infty}^{\infty} A(\omega)\, \mathrm{e}^{\mathrm{i}k(\omega)r\cos(\theta-\theta_I)-\mathrm{i}\omega t}\, \mathrm{d}\omega, \tag{3.8}$$

which represents unidirectional plane waves with the random amplitude spectrum A, with r, θ being the polar coordinates and θ_I the incident angle. Note that $A^*(\omega) = A(-\omega)$ since ζ_I is real. For each frequency ω, the wavenumber $k(\omega)$ is given by the dispersion relation,

$$\omega^2 = gk \tanh kh. \tag{3.9}$$

At the leading order, the correlation function of the incident waves is

$$H_2^I(\boldsymbol{x}, \tau) = \overline{\zeta_1^{(I)}(\boldsymbol{x}, t)\, \zeta_1^{(I)^*}(\boldsymbol{x}, t+\tau)} = \int_{-\infty}^{\infty} S_I(\boldsymbol{x}, \omega_2)\, \mathrm{e}^{\mathrm{i}\omega_2\tau}\, \mathrm{d}\omega_2 \tag{3.10}$$

where

$$S_I(\boldsymbol{x}, \omega_2) = \int_{-\infty}^{\infty} \overline{A(\omega_1)A^*(\omega_2)}\, \mathrm{e}^{\mathrm{i}[k(\omega_1)-k(\omega_2)]r\cos(\theta-\theta_I)-\mathrm{i}(\omega_1-\omega_2)t}\, \mathrm{d}\omega_1. \tag{3.11}$$

Due to the assumption of stationarity, we must have

$$\overline{A(\omega_1)A^*(\omega_2)} = S_A(\omega_1)\, \delta(\omega_1 - \omega_2), \tag{3.12}$$

which implies homogeneity, where $S_A(\omega)$ is the two-sided frequency spectrum. It follows that $S_I(\boldsymbol{x}, \omega_2) = S_I(\omega_2) \equiv S_A(\omega)$ is independent of space and

$$H_2^I(\boldsymbol{x}, \tau) = \int_{-\infty}^{\infty} S_A(\omega_2)\, \mathrm{e}^{\mathrm{i}\omega_2\tau}\, \mathrm{d}\omega_2. \tag{3.13}$$

Since H_2^I is real, S_A must be symmetric, i.e., $S_A(\omega_2) = S_A(-\omega_2)$.

Because of the complex bathymetry and lateral boundaries, diffraction and refraction affect the free-surface displacement near the scatterers. By linearity one expects the total first-order displacement to be of the form

$$\zeta_1(x, y, t) = \int_{-\infty}^{\infty} A(\omega)\, \Gamma_1(x, y, \omega)\, \mathrm{e}^{-\mathrm{i}\omega t}\, \mathrm{d}\omega, \tag{3.14}$$

where the frequency response (transfer function) Γ_1 will be found from the linear scattering theory. The following relation holds:

$$S_2(x, y, \omega) = S_A(\omega)\, |\Gamma_1(x, y, \omega)|^2, \tag{3.15}$$

as in all linearized time-invariant problems. Since ζ_1 is real and $A(\omega) = A^*(-\omega)$, we must have

$$\Gamma_1^*(x, y, \omega) = \Gamma_1(x, y, -\omega). \tag{3.16}$$

Following Sclavounos, we begin with the following formal expressions for the free-surface displacement at $O(\epsilon^2)$:

$$\zeta_2(x, y, t) = \iint_{-\infty}^{\infty} A(\omega_1)A(\omega_2)\, \Gamma_2(x, y, \omega_1, \omega_2)\, \mathrm{e}^{-\mathrm{i}(\omega_1+\omega_2)t}\, \mathrm{d}\omega_1\, \mathrm{d}\omega_2, \tag{3.17}$$

and at $O(\epsilon^3)$,

$$\zeta_3(x, y, t) = \iiint_{-\infty}^{\infty} A(\omega_1)A(\omega_2)A(\omega_3)\,\Gamma_3(x, y, \omega_1, \omega_2, \omega_3)\,\mathrm{e}^{-\mathrm{i}(\omega_1+\omega_2+\omega_3)t}\,\mathrm{d}\omega_1\,\mathrm{d}\omega_2\,\mathrm{d}\omega_3 \tag{3.18}$$

where $\Gamma_2(x, y, \omega_1, \omega_2)$ and $\Gamma_3(x, y, \omega_1, \omega_2, \omega_3)$ are the transfer functions yet unknown.

From (3.17) and (3.5), we get

$$H_{22} = \iiint_{-\infty}^{\infty} \mathrm{d}\omega_1\,\mathrm{d}\omega_2\,\mathrm{d}\omega_3\,\mathrm{d}\omega_4 \overline{A(\omega_1)A(\omega_2)A^*(\omega_3)A^*(\omega_4)} \times \Gamma_2(x, y, \omega_1, \omega_2)\,\Gamma_2^*(x, y, \omega_3, \omega_4)\,\mathrm{e}^{-\mathrm{i}(\omega_1+\omega_2-\omega_3-\omega_4)t}\,\mathrm{e}^{\mathrm{i}(\omega_3+\omega_4)\tau}. \tag{3.19}$$

By invoking Gaussianity,

$$\overline{A(\omega_1)A(\omega_2)A^*(\omega_3)A^*(\omega_4)} = \overline{A(\omega_1)A(\omega_2)}\quad\overline{A^*(\omega_3)A^*(\omega_4)} + \overline{A(\omega_1)A^*(\omega_3)}\quad\overline{A(\omega_2)A^*(\omega_4)} + \overline{A(\omega_1)A^*(\omega_4)}\quad\overline{A(\omega_2)A^*(\omega_3)} \tag{3.20}$$

and with repeated use of $A(\omega) = A^*(-\omega)$ and with (3.12), we find

$$\begin{aligned}\overline{A(\omega_1)A(\omega_2)A^*(\omega_3)A^*(\omega_4)} &= S_A(\omega_1)\delta(\omega_1+\omega_2)\,S_A(\omega_3)\,\delta(\omega_3+\omega_4) + S_A(\omega_1)\delta(\omega_1-\omega_3)\,S_A(\omega_2)\,\delta(\omega_2-\omega_4)\\ &\quad + S_A(\omega_1)\delta(\omega_1-\omega_4)\,S_A(\omega_2)\,\delta(\omega_2-\omega_3).\end{aligned} \tag{3.21}$$

Because of the delta functions, all four-fold integrals in (3.19) can be simplified to either single or double integrals, yielding finally,

$$\begin{aligned}H_{22}(x, y, \tau) &= \left[\int_{-\infty}^{\infty} S_A(\omega_1)\Gamma_2(x, y, \omega_1, -\omega_1)\,\mathrm{d}\omega_1\right]^2\\ &\quad + \int_{-\infty}^{\infty}\int_{-\infty}^{\infty} S_A(\omega_1)S_A(\omega_2)\{\Gamma_2(x, y, \omega_1, \omega_2)\,\Gamma_2^*(x, y, \omega_1, \omega_2)\\ &\quad + \Gamma_2(x, y, \omega_1, \omega_2)\,\Gamma_2^*(x, y, \omega_2, \omega_1)\}\mathrm{e}^{\mathrm{i}(\omega_1+\omega_2)\tau}\,\mathrm{d}\omega_1\,\mathrm{d}\omega_2.\end{aligned} \tag{3.22}$$

With the transformation

$$\omega = \omega_1 + \omega_2, \tag{3.23}$$

(3.22) becomes, after hiding the spatial dependence,

$$H_{22}(\tau) = \int_{-\infty}^{\infty} \mathrm{d}\omega \mathrm{e}^{\mathrm{i}\omega\tau}\delta(\omega)[\bar{\zeta}_2]^2 + \int_{-\infty}^{\infty} \mathrm{d}\omega\,\mathrm{e}^{\mathrm{i}\omega\tau}\int_{-\infty}^{\infty} S_A(\omega_1)S_A(\omega-\omega_1)\Gamma_2(\omega_1, \omega-\omega_1) \times [\Gamma_2^*(\omega_1, \omega-\omega_1) + \Gamma_2^*(\omega-\omega_1, \omega_1)]\,\mathrm{d}\omega_1. \tag{3.24}$$

By Fourier transform, the corresponding frequency spectrum is

$$S_{22}(\omega) = \delta(\omega)[\bar{\zeta}_2]^2 + \mathscr{I}(\omega) \tag{3.25}$$

where $\mathscr{I}$ denotes the integral:

$$\begin{aligned}\mathscr{I}(\omega) &= \int_{-\infty}^{\infty} S_A(\omega_1)S_A(\omega-\omega_1)\Gamma_2(\omega_1, \omega-\omega_1)[\Gamma_2^*(\omega_1, \omega-\omega_1) + \Gamma_2^*(\omega-\omega_1, \omega_1)]\,\mathrm{d}\omega_1\\ &= \int_{-\infty}^{\infty} S_A(\omega_1)S_A(\omega_2)\,\Gamma_2(\omega_1, \omega_2)\,[\Gamma_2^*(\omega_1, \omega_2) + \Gamma_2^*(\omega_2, \omega_1)]\,\mathrm{d}\omega_1.\end{aligned} \tag{3.26}$$

where ω_1 and ω_2 are related by (3.23). The first term in (3.25) corresponds to the square of the mean sea level; this quantity is usually not available from field data, as

indicated by figure 1, due probably to limits of instrumentation, and can be affected by tides. Since our focus is limited to low frequencies (small ω), the remaining integral $\mathscr{I}$ can be evaluated by first obtaining the transfer function $\Gamma_2(x, y, \omega_1, \omega_2)$ only in a narrow strip near the diagonal $\omega_1 + \omega_2 = 0$ instead of the entire plane of ω_1, ω_2. This is fortunate since it will reduce the computational efforts significantly.

For later computation of $\mathscr{I}$, the integration variable ω_1 is replaced by $-\omega_1$ over the interval $[-\infty, 0]$. Making use of $S_A(\omega_1) = S_A(-\omega_1)$, (3.26) can be written as a one-sided integral

$$\mathscr{I}(\omega) = \int_0^\infty S_A(\omega_1)\{S_A(\omega-\omega_1)\Gamma_2(\omega_1, \omega-\omega_1)[\Gamma_2^*(\omega_1, \omega-\omega_1) + \Gamma_2^*(\omega-\omega_1, \omega_1)] + S_A(\omega+\omega_1)\Gamma_2(-\omega_1, \omega+\omega_1)[\Gamma_2^*(-\omega_1, \omega+\omega_1) + \Gamma_2^*(\omega+\omega_1, -\omega_1)]\}\,\mathrm{d}\omega_1. \quad (3.27)$$

By steps similar to those leading to (3.22), H_{13} is found to be

$$H_{13}(x, y, \tau) = \int_{-\infty}^\infty \mathrm{d}\omega_1\, \mathrm{e}^{\mathrm{i}\omega_1\tau} S_A(\omega_1)\Gamma_1(x, y, \omega_1)\left\{\int_{-\infty}^\infty S_A(\omega_2)[\Gamma_3^*(x, y, \omega_1, \omega_2, -\omega_2) + \Gamma_3^*(x, y, \omega_2, \omega_1, -\omega_2) + \Gamma_3^*(x, y, \omega_2, -\omega_2, \omega_1)]\,\mathrm{d}\omega_2\right\}. \quad (3.28)$$

The corresponding frequency spectrum S_{13} is, after replacing ω_1 by ω,

$$S_{13}(\omega) = S_A(\omega)\Gamma_1(\omega)\int_{-\infty}^\infty S_A(\omega_2)[\Gamma_3^*(x, y, \omega, \omega_2, -\omega_2) + \Gamma_3^*(x, y, \omega_2, \omega, -\omega_2) + \Gamma_3^*(x, y, \omega_2, -\omega_2, \omega)]\,\mathrm{d}\omega_2. \quad (3.29)$$

Furthermore,

$$H_{31}(x, y, \tau) = \int_{-\infty}^\infty \mathrm{d}\omega_1\, \mathrm{e}^{\mathrm{i}\omega_1\tau}\left\{S_A(\omega_1)\Gamma_1^*(x, y, \omega_1)\int_{-\infty}^\infty S_A(\omega_2)[\Gamma_3(x, y, \omega_1, \omega_2, -\omega_2) + \Gamma_3(x, y, \omega_2, \omega_1, -\omega_2) + \Gamma_3(x, y, \omega_2, -\omega_2, \omega_1)]\,\mathrm{d}\omega_2\right\}. \quad (3.30)$$

The dependence on x, y is omitted on the right for brevity. The corresponding frequency spectrum is

$$S_{31}(x, y, \omega) = S_A(\omega)\Gamma_1^*(x, y, \omega)\int_{-\infty}^\infty S_A(\omega_2)[\Gamma_3(x, y, \omega, \omega_2, -\omega_2) + \Gamma_3(x, y, \omega_2, \omega, -\omega_2) + \Gamma_3(x, y, \omega_2, -\omega_2, \omega)]\,\mathrm{d}\omega_2. \quad (3.31)$$

In summary, the nonlinear spectral correction S_4 is the sum of (3.25), (3.29) and (3.31). In principle, the main task is to find the transfer functions Γ_1, Γ_2 and Γ_3 which are associated with the first-, second- and third-order diffraction, and, if the sea depth is slowly varying, refraction also. For simple plane standing waves in deep water, Sclavounos derived explicitly these transfer functions and calculated S_{22}, S_{13} and S_{31} for all frequencies $0 < \omega < \infty$ after taking the JONSWAP spectrum for S_A. For complex bathymetry and geometry, the tasks of computing $\Gamma_2(x, y; \omega_1, \omega_2)$ for all pairs of frequencies in the (ω_1, ω_2)-plane, and analyzing and computing $\Gamma_3(x, y; \omega_1, \omega_2, \omega_3)$ for all ω_i are prohibitive.

In typical sea spectra such as JONSWAP and their extension to finite water depth (see figure 3), $S_A(\omega)$ is practically zero for small ω. In view of relation (3.15),

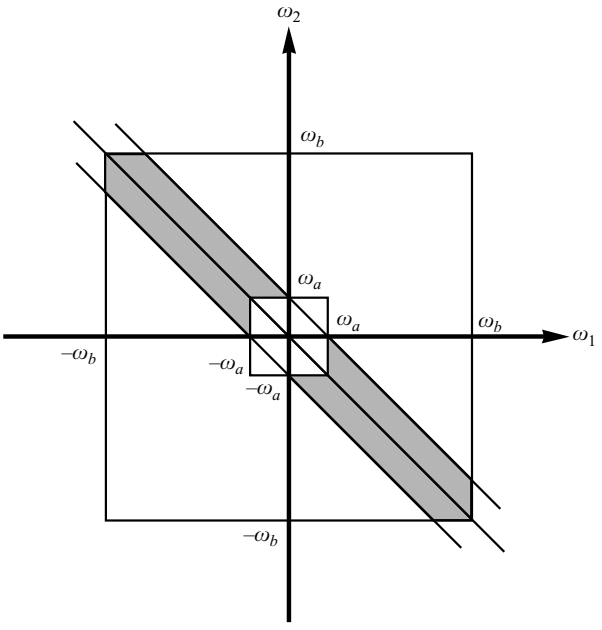

FIGURE 2. Plane of (ω_1, ω_2). Γ_2 is computed for frequency pairs inside the shaded strips. Frequencies ω_a and ω_b are the truncated limits of the incident sea spectrum.

the leading-order harbour response $S_2(x, y, \omega)$ is virtually zero in the low-frequency range, where the total spectrum is dominated by the nonlinear correction S_4. Since $S_{13}(x, y, \omega)$ and $S_{31}(x, y, \omega)$ are in direct proportion to $S_A(x, y, \omega)$, they must also be negligibly small at low frequencies. This result makes it unnecessary to compute Γ_3 or ζ_3 to obtain S_4, for small ω. On the other hand, $S_{22}(x, y, \omega)$ is not proportional to $S_A(\omega)$ but depends on it through a convolution integral in (3.26). Thus $S_{22}(x, y, \omega)$ is not necessarily zero when $S_A(\omega)$ vanishes. It would appear at first sight that one must find the second-order transfer function $\Gamma_2(x, y, \omega_1, \omega_2)$ for many (in principle, infinite) pairs of frequencies to cover nearly the entire plane of (ω_1, ω_2). Fortunately our interest is in the low-frequency response, i.e. small ω. Hence $\Gamma_2(x, y, \omega_1, \omega_2)$ is needed only for frequency pairs in a narrow strip near the diagonal $\omega_1 + \omega_2 = 0$. In numerical computations, the incident sea spectrum $S_A(\omega)$ can be truncated so that it is non-zero only in a finite range $\omega_a < \omega < \omega_b$. Thus, only the pairs in the shaded portions of the narrow strip shown in figure 2 are relevant. These two advantages are particularly suited to the harbour resonance problem (and to slow-drift problems of ships and floating platforms). In the range of high frequencies, contributions by S_{22}, S_{13} and S_{31} are of $O(\epsilon^4)$ importance but are all much smaller than $S_2 = O(\epsilon^2)$; these corrections are not pursued here.

We now turn to the transfer functions $\Gamma_1(x, y, \omega)$ and $\Gamma_2(x, y, \omega_1, \omega_2)$.

4. First-order transfer function

Let the first-order velocity potential be represented by the Fourier–Stieltjes integral

$$\Phi_1(\boldsymbol{x}, t) = \int_{-\infty}^{\infty} A(\omega)\, \phi_1(\boldsymbol{x}, \omega)\, \mathrm{e}^{-\mathrm{i}\omega t}\, \mathrm{d}\omega, \tag{4.1}$$

where $\boldsymbol{x} = (x, y, z)$. It follows from the first-order perturbation equations for Φ_1 that the first-order frequency response ϕ_1 is governed by

$$\left(\nabla_2^2 + \frac{\partial^2}{\partial z^2}\right)\phi_1(\boldsymbol{x}, \omega) = 0, \quad -h(x, y) < z < 0, \tag{4.2}$$

$$\frac{\partial \phi_1(\boldsymbol{x}, \omega)}{\partial z} = -\nabla_2 \phi_1(\boldsymbol{x}, \omega) \cdot \nabla_2 h, \quad z = -h(x, y), \tag{4.3}$$

$$\frac{\partial \phi_1(\boldsymbol{x}, \omega)}{\partial z} - \frac{\omega^2}{g}\phi_1(\boldsymbol{x}, \omega) = 0, \quad z = 0. \tag{4.4}$$

For slowly varying depth this diffraction problem is in general three-dimensional. An efficient approximation is the well-known mild-slope equation which involves only two horizontal dimensions as in the limiting case of constant depth. The plane diffraction problem in (x, y) can be numerically solved by the hybrid-element method. Specifically, by assuming the potential to be dominated by the propagating mode,

$$\phi_1(x, \omega) = -\frac{\mathrm{i}g}{\omega}\frac{\cosh[k(\omega)(z+h)]}{\cosh[k(\omega)h]}\Gamma_1(x, y, \omega), \tag{4.5}$$

$\Gamma_1(x, y, \omega)$ is shown to be governed by the two-dimensional mild-slope equation of Chamberlain & Porter (1995). The associated elliptic boundary-value problem can be solved by the hybrid-element method of Chen & Mei (1974).

5. Second-order transfer function

5.1. *The potential*

At the second order, Φ_2 satisfies the three-dimensional Laplace equation and the seabed condition (2.3). Let us rewrite the inhomogeneous free-surface boundary condition as

$$\frac{\partial \Phi_2}{\partial z} + \frac{1}{g}\frac{\partial^2 \Phi_2}{\partial t^2} = F, \quad z = 0, \tag{5.1}$$

where

$$F = \frac{1}{g^2}\frac{\partial \Phi_1}{\partial t}\frac{\partial}{\partial z}\left[g\left(\frac{\partial \Phi_1}{\partial z}\right) + \frac{\partial^2 \Phi_1}{\partial t^2}\right] - \frac{1}{g}\frac{\partial}{\partial t}(\nabla_3 \Phi_1)^2, \quad z = 0. \tag{5.2}$$

With (4.1), the forcing function F becomes

$$F = \iint_{-\infty}^{\infty} A(\omega_1)A(\omega_2) f(x, y, \omega_1, \omega_2)\, \mathrm{e}^{-\mathrm{i}(\omega_1+\omega_2)t}\, \mathrm{d}\omega_1\, \mathrm{d}\omega_2 \tag{5.3}$$

where

$$f(x, y, \omega_1, \omega_2) = \left\{-\frac{\mathrm{i}\omega_1}{g}\phi_1(x, \omega_1)\left[\frac{\partial^2 \phi_1(x, \omega_2)}{\partial z^2} - \frac{\omega_2^2}{g}\frac{\partial \phi_1(x, \omega_2)}{\partial z}\right] + \frac{\mathrm{i}(\omega_1+\omega_2)}{g}\nabla_3 \phi_1(x, \omega_1) \cdot \nabla_3 \phi_1(x, \omega_2)\right\}_{z=0}. \tag{5.4}$$

Putting (4.5) into (5.4), we obtain

$$f(x, y, \omega_1, \omega_2) = \beta_1(\omega_1, \omega_2)\Gamma_1(x, y, \omega_1)\Gamma_1(x, y, \omega_2) + \beta_2(\omega_1, \omega_2)\nabla_2 \Gamma_1(x, y, \omega_1) \cdot \nabla_2 \Gamma_1(x, y, \omega_2) \tag{5.5}$$

with

$$\beta_1(\omega_1,\omega_2)=\frac{\mathrm{i}g\,[k(\omega_2)]^2}{\omega_2}-\frac{\mathrm{i}\omega_2^3}{g}-\frac{\mathrm{i}(\omega_1+\omega_2)\,\omega_1\omega_2}{g}, \tag{5.6}$$

and

$$\beta_2(\omega_1,\omega_2)=-\frac{\mathrm{i}(\omega_1+\omega_2)\,g}{\omega_1\omega_2}. \tag{5.7}$$

Unlike the monochromatic case studied in Chen & Mei (2006), the forcing function here depends on two frequencies. Note for later use that if $\omega_1+\omega_2=0$,

$$\beta_1(\omega_1,-\omega_1)=-\beta_1(-\omega_1,\omega_1),\quad \beta_2(\omega_1,-\omega_1)=\beta_2(-\omega_1,\omega_1)=0,$$

which implies

$$f(\omega_1,-\omega_1)=-f(-\omega_1,\omega_1). \tag{5.8}$$

Let us express the second-order potential in the form

$$\Phi_2(\boldsymbol{x},t)=\iint_{-\infty}^{\infty}A(\omega_1)A(\omega_2)\,\phi_2(\boldsymbol{x},\omega_1,\omega_2)\,\mathrm{e}^{-\mathrm{i}(\omega_1+\omega_2)t}\,\mathrm{d}\omega_1\,\mathrm{d}\omega_2. \tag{5.9}$$

Putting (5.9) into (2.2), (2.3) and (2.6), we find that $\phi_2(\boldsymbol{x},\omega_1,\omega_2)$ satisfies the same conditions (4.2) and (4.3) as ϕ_1, and the inhomogeneous free-surface boundary condition,

$$\frac{\partial\phi_2}{\partial z}-\frac{(\omega_1+\omega_2)^2}{g}\phi_2=f(x,y,\omega_1,\omega_2),\qquad z=0. \tag{5.10}$$

Together with the weak radiation condition, (2.2), (2.3), (2.4) and (5.10) form the second-order boundary value problem.

As in the case of monochromatic waves (Chen & Mei 2006), we assume the second-order potential $\phi_2(\boldsymbol{x},\omega_1,\omega_2)$ to take the form

$$\phi_2(\boldsymbol{x},\omega_1,\omega_2)=-\frac{\mathrm{i}g}{\omega_1+\omega_2}\sum_{m=0}^{\infty}\xi_m(x,y,\omega_1,\omega_2)\,\frac{\cos\kappa_m(z+h)}{\cos\kappa_m h}, \tag{5.11}$$

where κ_m, $m=1,2,\ldots$ are the real roots of the equation

$$-(\omega_1+\omega_2)^2=g\kappa_m\tan\kappa_m h,\quad (m-1/2)\,\pi\leqslant\kappa_m h\leqslant m\pi, \tag{5.12}$$

and κ_0 is imaginary

$$\kappa_0=-\mathrm{i}\widehat{\kappa}_0, \tag{5.13}$$

with $\widehat{\kappa}_0$ being the real root of the dispersion equation

$$(\omega_1+\omega_2)^2=g\widehat{\kappa}_0\tanh\widehat{\kappa}_0 h. \tag{5.14}$$

Here $m=0$ represents the propagating mode in which the waves propagate to infinity, while $m\geqslant 1$ represent the evanescent modes localized near the scatterers. Applying the vertical averaging procedure as for the mild-slope equation at the first order, we obtain a coupled set of modified mild-slope equations for $\xi_\ell(x,y,\omega_1,\omega_2)$. Since the procedure of derivation is identical to that for the limiting case of monochromatic waves in Chen & Mei (2006), only the results are given:

$$\sum_{\ell=0}^{\infty}\{\nabla\cdot[A_{m,\ell}\nabla\xi_\ell]+B_{m,\ell}\nabla\xi_\ell\cdot\nabla h+C_{m,\ell}\xi_\ell\}$$
$$=-\mathrm{i}(\omega_1+\omega_2)\,f(x,y,\omega_1,\omega_2),\quad m=0,1,2,3,\ldots \tag{5.15}$$

where

$$A_{m,\ell} = \frac{gh}{2\cos^2\kappa_\ell h}\left(1 + \frac{\sin 2\kappa_\ell h}{2\kappa_\ell h}\right)\delta_{m\ell} \tag{5.16}$$

is diagonal;

$$B_{m,\ell} = \begin{cases} 0, & \text{when } m = \ell \\ g(U_{m,\ell} - U_{\ell,m}), & \text{when } m \neq \ell \end{cases} \tag{5.17}$$

with

$$U_{m,\ell} = \begin{cases} \dfrac{\sin 2\kappa_m h - 2\kappa_m h\cos 2\kappa_m h}{4\cos^2(\kappa_m h)\,(2\kappa_m h + \sin 2\kappa_m h)}, & \text{when } m = \ell, \\ -\dfrac{\kappa_\ell^2}{\left(\kappa_\ell^2 - \kappa_m^2\right)\cos\kappa_m h\cos\kappa_{n,l} h}, & \text{when } m \neq \ell, \end{cases} \tag{5.18}$$

and

$$C_{m,\ell} = -\kappa_m^2 A_{m,\ell} + gU_{m,\ell}\nabla^2 h + gV_{m,\ell}\,(\nabla h)^2\,. \tag{5.19}$$

The expressions for $V_{m,\ell}$ are, for $m = \ell$,

$$V_{m,m} = \frac{-\kappa_m \sec^2(\kappa_m h)}{12(2\kappa_m h + \sin 2\kappa_m h)^3}[(2\kappa_m h)^4 + 4(2\kappa_m h)^3\sin 2\kappa_m h + 9\sin(2\kappa_m h)\sin 4\kappa_m h \\ - 12\kappa_m h(\kappa_m h + \sin 2\kappa_m h)(\cos^2 2\kappa_m h - 2\cos 2\kappa_m h + 3)], \tag{5.20}$$

and for $m \neq \ell$,

$$V_{m,\ell} = \frac{-2\kappa_\ell \sec\kappa_m h\sec\kappa_\ell h}{(2\kappa_\ell h + \sin 2\kappa_\ell h)}\frac{\left[4\kappa_\ell^2\kappa_m^2 + \left(\kappa_\ell^4 - \kappa_m^4\right)\sin^2\kappa_\ell h\right]}{\left(\kappa_\ell^2 - \kappa_m^2\right)^2}. \tag{5.21}$$

Equation (5.15) forms a matrix equation and $C_{m,\ell}$ contains $O(\mu^0)$, $O(\mu)$, and $O(\mu^2)$ terms where $\mu \equiv O(\nabla h/kh) \ll 1$. The unknowns ξ_ℓ, $\ell = 0, 1, 2, 3, \ldots$, must be solved subject to the usual no-flux condition on lateral walls, and the weak radiation condition at infinity.

For later use we note that if $\omega_1 + \omega_2 = 0$, the forcing term in (5.15) vanishes, hence

$$\xi_\ell(\omega_1, -\omega_1) \equiv 0, \quad \ell = 0, 1, 2, 3, \ldots. \tag{5.22}$$

If the complex harbour geometry and variable bathymetry are limited to a finite region, the two-dimensional hybrid element analysis described in Chen & Mei (2006) for monochromatic incident waves can be applied to solve the coupled problems for $\xi_\ell(x, y, \omega_1, \omega_2)$, $\ell = 0, 1, 2, 3, \ldots$, for each frequency pair ω_1, ω_2.

In the limit of constant depth everywhere, (5.15) becomes a set of uncoupled two-dimensional Helmholtz equations,

$$\nabla^2\xi_\ell - \kappa_\ell^2\xi_\ell = -\mathrm{i}\frac{(\omega_1 + \omega_2)}{A_{\ell,\ell}}f, \quad \ell = 0, 1, 2, 3, \ldots. \tag{5.23}$$

Each ξ_ℓ can be solved separately by the two-dimensional hybrid-element method. The potential amplitude ϕ_2 and hence Φ_2 are then solved.

From (2.8), (2.9) and (2.10), the frequency-response function of the second-order free-surface elevation defined in (3.17) can be calculated according to

$$\begin{aligned}\Gamma_2(x, y, \omega_1, \omega_2) &= -\frac{\omega_1\omega_2}{g^2}\phi_1(x, \omega_1)\frac{\partial\phi_1(x, \omega_2)}{\partial z} - \frac{1}{2g}\nabla_3\phi_1(x, \omega_1)\cdot\nabla_3\phi_1(x, \omega_2)\\ &\quad + \frac{\mathrm{i}\sigma}{g}\phi_2(x, \omega_1, \omega_2)\\ &= \left(\frac{\omega_2^2}{g} + \frac{\omega_1\omega_2}{2g}\right)\Gamma_1(\omega_1)\Gamma_1(\omega_2) + \frac{g}{2\omega_1\omega_2}\nabla_2\Gamma_1(\omega_1)\cdot\nabla_2\Gamma_1(\omega_2)\\ &\quad + \sum_{\ell=0}^{\infty}\xi_\ell(\omega_1, \omega_2) \end{aligned} \tag{5.24}$$

which will be used to find the spectrum S_{22}.

6. The mean sea level

Using (5.24) in (3.17) and taking the ensemble average, we obtain the mean sea level

$$\begin{aligned}\overline{\zeta_2}(x) &= \int_{-\infty}^{\infty} S_A(\omega_1)\Gamma_2(x, y, \omega_1, -\omega_1)\,\mathrm{d}\omega_1\\ &= \int_0^{\infty} S_A(\omega_1)\left[\Gamma_2(x, y, \omega_1, -\omega_1) + \Gamma_2(x, y, -\omega_1, \omega_1)\right]\mathrm{d}\omega_1. \end{aligned} \tag{6.1}$$

However, there is no contribution to the last integral from the series in (5.24) since $\xi_\ell(\omega_1, -\omega_1)$ vanishes identically as noted in (5.22). Furthermore, since $\Gamma_1(-\omega_1) = \Gamma_1^*(\omega_1)$,

$$\begin{aligned}\Gamma_2(x, y, \omega_1, -\omega_1) &= \frac{\omega_1^2}{2g}\Gamma_1(\omega_1)\Gamma_1^*(\omega_1) - \frac{g}{2\omega_1^2}\nabla_2\Gamma_1(\omega_1)\cdot\nabla_2\Gamma_1^*(\omega_1).\\ &= \Gamma_2(x, y, -\omega_1, \omega_1). \end{aligned} \tag{6.2}$$

It follows finally that

$$\overline{\zeta_2}(x) = \int_0^{\infty} S_I(\omega_1)\left[\frac{{\omega_1}^2}{g}\Gamma_1(\omega_1)\Gamma_1^*(\omega_1) - \frac{g}{\omega_1^2}\nabla_2\Gamma_1(\omega_1)\cdot\nabla_2\Gamma_1^*(\omega_1)\right]\mathrm{d}\omega_1 \tag{6.3}$$

which depends only on the first-order potential.

7. Numerical examples

We shall adopt the TMA spectrum as our one-sided spectrum $2S_A$ of the incident sea. TMA refers to the sites where wave data were collected to derive this spectrum: TEXEL and MARSEN in the North Sea, and ARSLOE at Duck, North Carolina. The TMA spectrum is a modified JONSWAP spectrum for shallow seas (Ochi 1998),

$$S_{TMA}(\omega) = S_{JWP}(\omega)\frac{\left(\omega^2 h/g\right)^3}{\tanh kh + kh\cosh^2 kh}, \quad \omega > 0, \tag{7.1}$$

where

$$S_{JWP}(\omega) = \alpha\frac{g^2}{\omega^5}\exp\left[-1.25\frac{\omega^4}{\omega_p^4}\right]\gamma\exp[-(\omega-\omega_p)^2/2(\sigma\omega_p)^2] \tag{7.2}$$

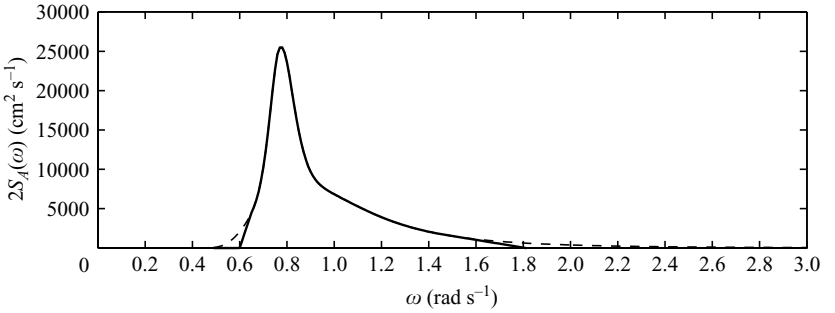

FIGURE 3. TMA spectrum. Dashed curve: calculated from (7.1) with inputs $h = 20\,\mathrm{m}$, $\bar{x} = 3000$ and $\bar{U} = 20\,\mathrm{m\,s^{-1}}$. Solid curve: truncated spectrum, $2S_A$ in our computations.

and ω and k are governed by the dispersion relation. The correction factor in (7.1) originally introduced for Phillips' spectrum is due to Kiatigorodskii, Krasitskii & Zaslavskii (1975). The empirical constants for the JONSWAP part are

$$\gamma = 3.3, \quad \alpha = 0.076\bar{x}^{-0.22}, \quad \sigma = \begin{cases} 0.07, & \omega < \omega_p, \\ 0.09, & \omega > \omega_p. \end{cases}$$

The dimensionless fetch $\bar{x}$ and the peak frequency ω_p are defined in terms of the wind speed $\bar{U}$ and fetch distance x according to

$$\bar{x} = gx/\bar{U}^2, \quad \omega_p = (2\pi)3.5(g/\bar{U})\bar{x}^{-0.33}.$$

In figure 3 the TMA spectrum is shown by the dashed curve for $\bar{U} = 20\ \mathrm{m\,s^{-1}}$ and $\bar{x} = 3000$ so that the peak frequency is $\omega_p = 0.767\,\mathrm{rad\,s^{-1}}$. To estimate the characterstic wave steepness ϵ we first compute the significant wave height according to

$$H_s = \sqrt{4\int_0^\infty 2S_A(\omega)\,\mathrm{d}\omega} \tag{7.3}$$

yielding the result $H_s = 1.85$ m. With the peak wavenumber $k_p = 0.068\,\mathrm{m^{-1}}$ found by the dispersion relation, the characteristic wave steepness is then $\epsilon = k_p H_s/2 = 0.063$. In our numerical computations the spectrum is truncated so that it is non-zero only within the range $0.6 < \omega < 1.8$, as shown by the solid curve. With reference to figure 2, the lower and upper cutoff frequencies are $\omega_b = 0.6\,\mathrm{rad\,s^{-1}}$ and $\omega_a = 1.8\,\mathrm{rad\,s^{-1}}$ respectively; the corresponding circular frequencies are $f_b = 3/10\pi\,\mathrm{Hz}$ and $f_a = 9/10\pi\,\mathrm{Hz}$.

A large part of the computational effort is of course the solution of the second-order diffraction problem for $\phi_2(x, y, z, \omega_1, \omega_2)$. While the three-dimensional problem is now reduced to two, the numerical computation of the two-dimensional modal amplitudes ξ_ℓ, $l = 0, 1, 2, 3, \ldots$, from the coupled equations (5.15) is still a demanding task in general, especially because computations must be repeated for many pairs of frequencies as shown in figure 2. An example of such a numerical task has been demonstrated only for monochromatic waves approaching a vertical cylinder on the top of a circular shoal (Chen & Mei 2006). In the limit of contant depth everywhere, the modes are uncoupled and the mild-slope equations for all modes can be solved separately. Since the primary mechanism of the harbour resonance is associated with sheltering by lateral boundaries, we shall limit our attention here to the simpler example of a small square harbour (300 m by 300 m) behind a straight coast in constant depth of 20 m. The hybrid-element method used in Chen & Mei (2006) is modified for both first- and second-order transfer functions.

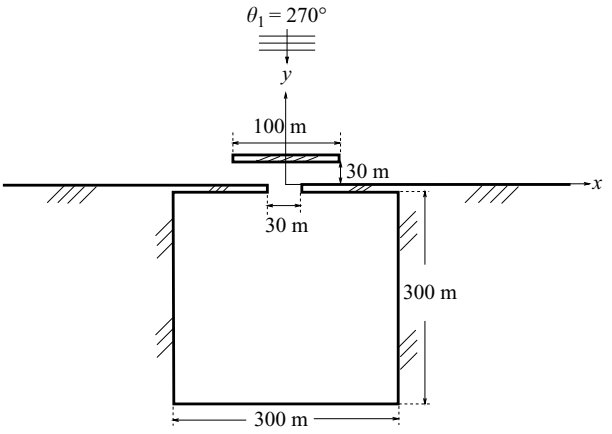

FIGURE 4. Plan view of a protected square basin (Case iii). For Cases (i) and (ii), the entrance widths are 60 m and 30 m respectively, without the detached breakwater.

It well-known in the linearized theory (Miles & Munk 1961) that, without accounting for frictional losses at the entrance, the resonance peaks in the plot of amplification vs. frequency are taller and thinner for the Helmholtz and the lowest modes if the entrance is narrower (the harbour paradox). To examine the possible nonlinear manifestations, three cases are considered for comparison: (i) a wide entrance (of width 60 m) open to the sea, (ii) a narrow entrance (of width 30 m) open to the sea, and (iii) a narrow entrance protected by a detached breakwater. The dimensions of Case (iii) are shown in figure 4. All breakwaters are of caisson type and 5 m thickness. Analytical solutions are used for the semi-infinite sea outside a semi-circle which is centred at the entrance and of radius (30 m, 15 m, and 62 m) for Cases ((i), (ii) and (iii)) respectively. Simple triangular elements are used to discretize the basin and the region within the semi-circle. The maximum element size is $L_e = 1$ m, so that $k_p L_e = 0.068$, or $L_e/\lambda_p = 0.0108$. The total number of nodes used is $N_p = (164\,062, 162\,935, 171\,209)$ for Cases ((i), (ii), (iii)) respectively. Only normal incidence ($\theta_I = 3\pi/2$) is considered.

In the computation of the double-integral in S_{22}, the main task is to compute the transfer function $\Gamma_2(\omega_1, \omega_2)$ at many points in the shaded strips in the plane of ω_1, ω_2, as shown in figure 2. With the frequency increment chosen to be $\Delta\omega, \Delta\omega_1, \Delta\omega_2 = 0.01\,\mathrm{rad\,s^{-1}}$, the strips within the range $0.6\,\mathrm{rad\,s^{-1}}, < \omega_1, \omega_2 < 1.8\,\mathrm{rad\,s^{-1}}$ are discretized. At each point, the hybrid-element method is needed and finite element matrix equations have to be solved numerically for ξ_ℓ. For each ω, i.e. along each diagonal line $\omega = \omega_1 + \omega_2$, the total number of points is at least 100. We have computed the solutions from $\omega = 0.01\,\mathrm{rad\,s^{-1}}$ to $0.6\,\mathrm{rad\,s^{-1}}$, hence the total number of points (ω_1, ω_2) needed for each mode is 10 620. The CPU time for solving each point is around 15 minutes. Using 20–25 personal computers in parallel, the total computational time for one of the three Cases is around two weeks.

7.1. *First order*

As an overall representation of the first-order effect, we first display in figure 5 the spatially averaged frequency response $\langle \Gamma_1(\omega) \rangle$ for all ω defined by

$$\langle \Gamma_1(\omega) \rangle = \left(\frac{1}{A_b} \iint_{A_b} |\Gamma_1(x, y, \omega)|^2 \, \mathrm{d}x \, \mathrm{d}y \right)^{1/2}, \quad 0 < \omega, \tag{7.4}$$

where A_b denotes the basin area.

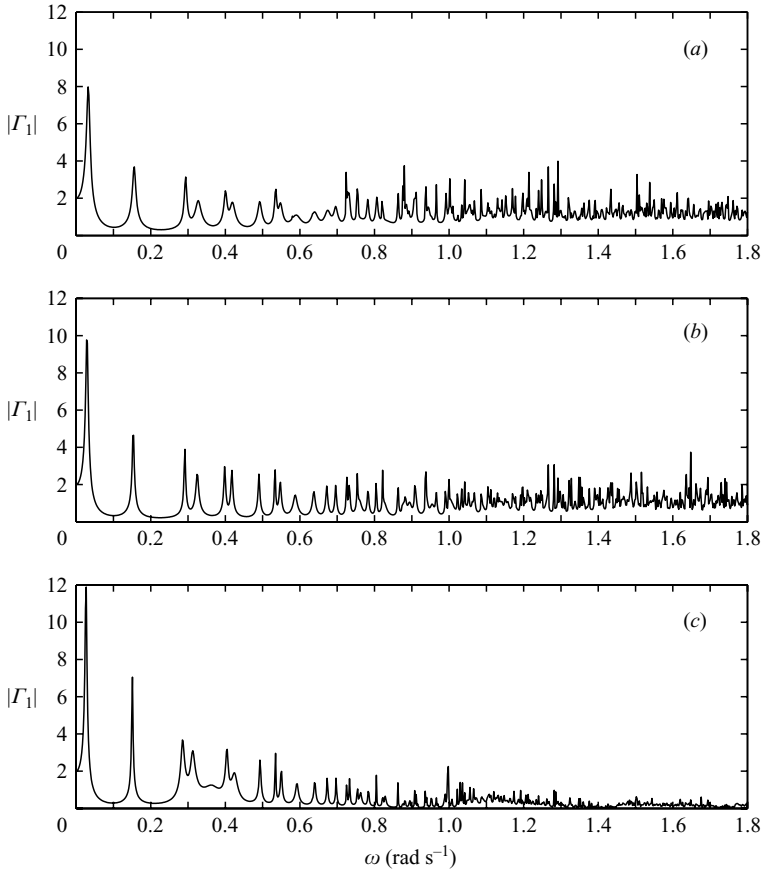

FIGURE 5. Basin-averaged first-order frequency response $\langle \Gamma_1(\omega) \rangle$: (*a*) opening 60 m, (*b*) 30 m, (*c*) 30 m with protection.

The lowest peaks, at frequencies $\omega = 0.032$ rad s^{-1}, $\omega = 0.028$ rad s^{-1} and $\omega = 0.027$ rad s^{-1} for Case (i), (ii) and (iii) respectively, correspond to the Helmholtz mode or pumping mode where the free surface within the harbour rises and falls in unison. The remaining non-Helmholtz modes have been identified as the natural modes of the closed basin,

$$\eta_{n,m} = a_{n,m} \cos\left[\frac{n\pi}{300}(x + 150)\right] \cos\left[\frac{m\pi}{300}(y + 305)\right]. \tag{7.5}$$

The greatest amplification occurs at the first (Helmholtz) peak. The heights of this and other low-frequency peaks ($\omega < 0.6$) are greater for the narrower entrance, a consequence of the harbour paradox, since friction is unaccounted for. On the other hand, the high-frequency peaks ($\omega > 0.6$) are lower for the narrower entrances. The detached breakwater reduces the high-frequency response even further. It should be pointed out that local responses at different stations may differ quantitatively from the average, especially if the station is situated at either a node or an antinode of a particular natural mode. The effects of the entrance geometry are, however, qualitatively the same.

The spatially averaged linear spectra $S_2(\omega)$ for three different entrances are shown in figure 6. Recall from relation (3.15) that $S_2(\omega)$ is proportional to the incident wave spectrum, hence is essentially zero for $\omega < 0.6$ and not plotted. It can be seen that

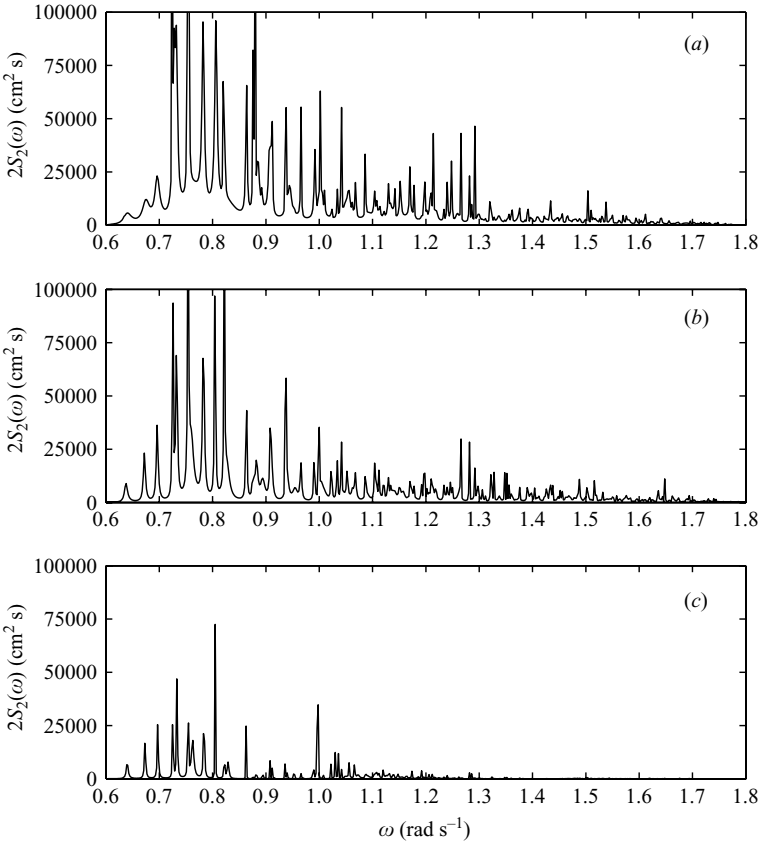

FIGURE 6. Basin-averaged first-order spectrum $S_2(\omega)$: (*a*) opening 60 m, (*b*) 30 m, (*c*) 30 m with protection. Only the high-frequency range is shown.

among the three entrances, the area under $S_2(\omega)$ is the largest for Case (i) and the smallest for Case (iii) From (7.3), contributions of the low-frequency spectral peaks to the significant wave heights H_s are 1.2 m, 0.8 m and 0.5 m for Cases (i) (ii) and (iii) respectively, obtained by calculating the area under the S_2 curve. All are of course less than $H_s = 1.85$ m of the incident waves.

7.2. *Nonlinear effects*

We now examine the nonlinear corrections. Figures 7(*a*), 7(*b*) and 7(*c*) give the mean-sea-level variations for three entrances. In general better protection at the entrance leads to lower maximum setup/setdown. According to (6.1), the mean-sea-level setup/setdown is an accumulated effect of various frequencies. To better understand the computed result, it is useful to describe the mean sea level as simple harmonic standing waves in the closed basin, described by (7.5),

$$\frac{\eta_{20}}{a_{n,m}^2} = \frac{\omega_{n,m}^2}{g}\left|\cos\left[\frac{n\pi}{300}(x+150)\right]\cos\left[\frac{m\pi}{300}(y+305)\right]\right|^2 - \frac{g}{\omega_{n,m}^2}\frac{n\pi}{300}\left\{\sin\left[\frac{n\pi}{300}(x+150)\right]\cos\left[\frac{m\pi}{300}(y+305)\right]\right\}^2 - \frac{g}{\omega_{n,m}^2}\frac{m\pi}{300}\left\{\cos\left[\frac{n\pi}{300}(x+150)\right]\sin\left[\frac{m\pi}{300}(y+305)\right]\right\}^2, \tag{7.6}$$

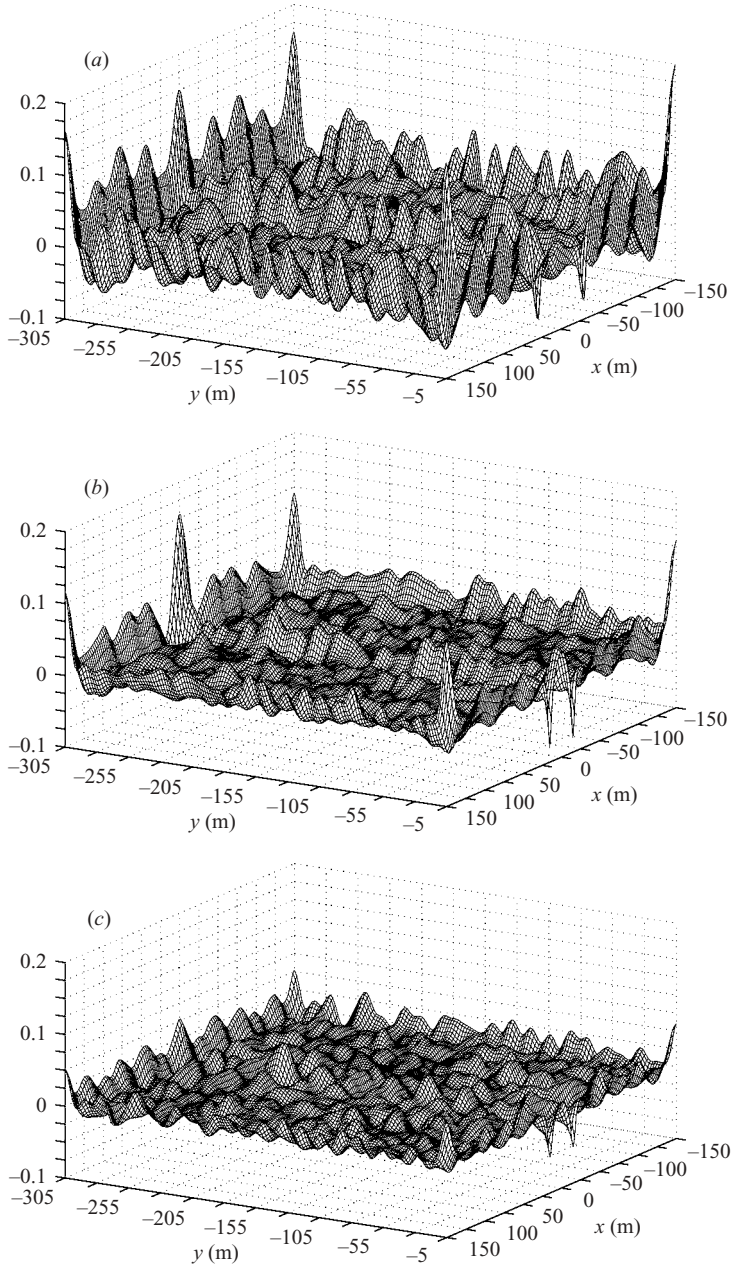

FIGURE 7. Setup/setdown for (*a*) wide entrance of width 60 m, (*b*) narrow entrance of width 30 m, (*c*) narrow entrance of 30 m width with breakwater.

which follows from the time average of (2.9). Since the most energetic modes are the first eight ($\omega_{n,m}$, with $(n, m) = (0, 5)$, $(2, 5)$, $(4, 4)$, $(0, 6)$, $(6, 1)$, $(4, 5)$, $(6, 3)$ and $(0, 7)$) which are all in the range of $0.6\,\mathrm{rad\,s^{-1}} < \omega < 1.8\,\mathrm{rad\,s^{-1}}$, they are the largest contributors to $\bar{\zeta}_2$. Due to the staggering of the nodal and antinodal lines, a combination of all these modes renders a very complex picture of the mean free surface in figure 7.

The basin-averaged low-frequency wave spectra obtained from $S_{22}(\omega)$ are shown in figure 8 for three entrances. The first two peaks in S_{22} correspond to the Helmholtz

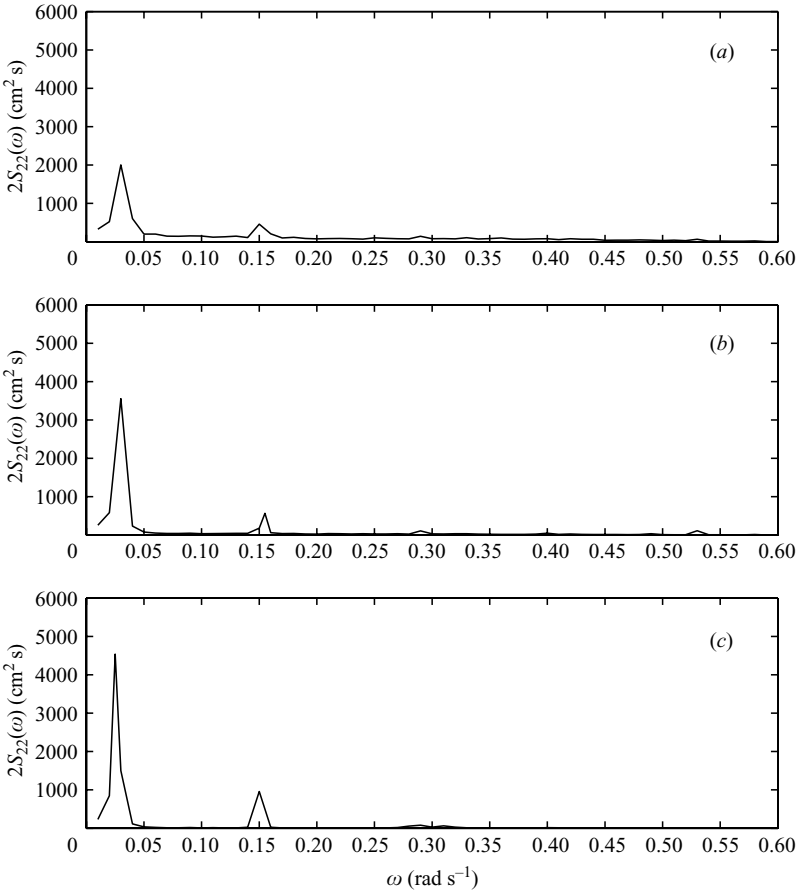

FIGURE 8. Basin-averaged nonlinear correction $2S_{22}(\omega)$ in the low-frequency range: (*a*) opening 60 m, (*b*) 30 m, (*c*) 30 m with protection.

mode and the first non-Helmholtz mode observed in the first-order response curves, with similar dependence on the opening. The phenomenon of the harbour paradox known in the first-order result is again observed. It can be seen that most of the low-frequency energy concentrates in the neighbourhood of the first two modes.

Despite the differences in geometry, qualitative comparisons can be made with the field data from Hualien Harbour during Typhoon Tim. As can be seen in figure 1, high-frequency peaks at inside Stations 8 and 10 are greatly reduced by a factor of $1/200$, due to the effective protection by the breakwater, but the low-frequency peaks are enhanced by a factor of a hundred.

For qualitative comparison of the computed result with the observed spectra during Typhoon Tim in Hualien Harbour, we present in figure 9 the composite spectrum $S(f) = S_2(f) \cup S_{22}(f)$ for both the low- and high-frequency ranges as a function of the circular frequency $f = \omega/2\pi$ Hz. In the high-frequency range ($3/10\pi < f < 9/10\pi$ Hz), S_2 is plotted without the correction for S_4. In the low-frequency range ($0 < f < 3/10\pi$ Hz), $S_{22} = S_4$ is shown instead. Use is made of the relation $S_f(f) = 2\pi S(\omega)$. The computed spectra bear strong qualitative resemblance to the records at Hualien Harbour. In particular the result for Case (iii) where the entrance is protected most is very similar to the observed spectra at the inside stations 8 and 10 far from the harbour entrance.

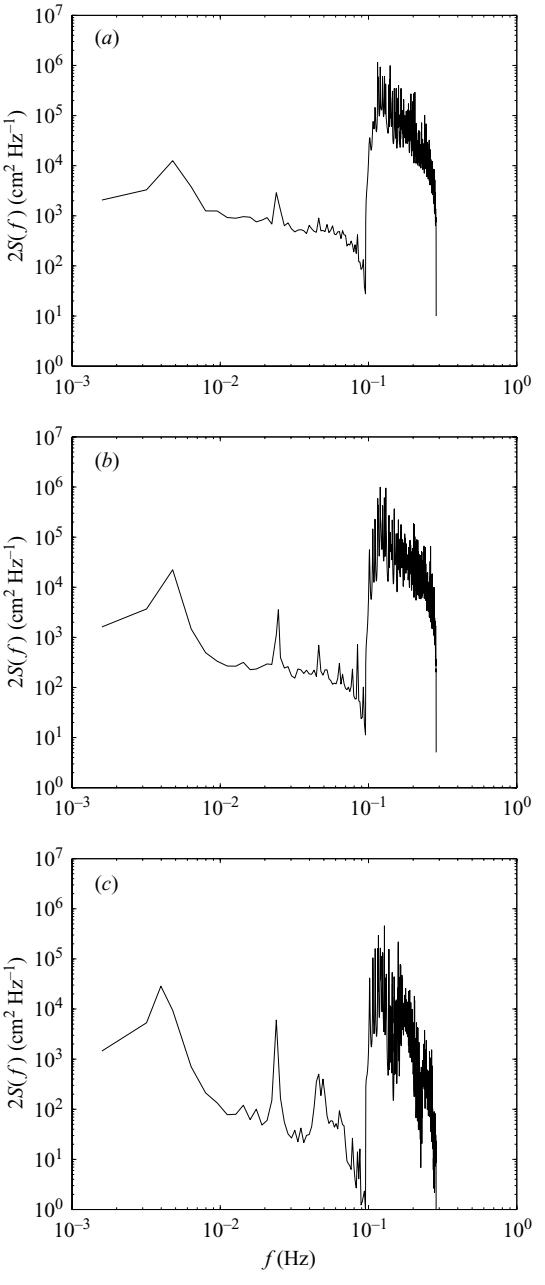

FIGURE 9. Spatial-averaged spectrum $2S(f)$ (Case i). High-frequency range: $2S(f) = 2S_2(f)$, $f > 3/10\pi$ Hz. Low-frequency range: $2S(f) = 2S_{22}(f)$, $f < 3/10\pi$ Hz. (*a*) for 60 m opening, (*b*) 30 m opening, (*c*) 30 m opening with breakwater.

8. Concluding remarks

In this article we have presented the theory of long-period resonance in a harbour by random short incident waves of a broad frequency band. Under the assumptions that the incident waves are stationary and Gaussian, the nonlinear correction to the response spectrum requires in principle the solution of not only the first- and second- but also the third-order diffraction problems. Thanks to a common feature

that coastal waves have negligible energy at low frequencies, the first two orders are sufficient for our purpose. The second-order mild-slope approximation recently reported by us is extended so that only two-dimensional discretization is need to solve the intrinsically three-dimensional diffraction problems. To examine the resonance in a partially enclosed region we treated an example of a small harbour in a sea of constant depth. In the high-frequency range, the harbour spectrum is lower than that of the incident waves, due to sheltering by breakwaters. In the low-frequency range outside the incident-wave spectrum, the harbour spectrum is much higher than that of the outside sea, due to the excitation of Helmholtz and other low-frequency standing wave modes.

Application of the present theory to natural harbours of large area and variable depth requires additional account of the directional distribution of the incident sea spectrum, and further streamlining of the computing algorithms, both of which are planned for the future. Changes of the spectral response due to the excitation of low-frequency edge waves and their influence on the harbour resonance should of course be of practical interest. Empirical models representing the breaking of short waves on a sloping beach must be incorporated into the stochastic theory. While the alternative of laboratory experiments is frequently chosen in harbour design, it is common experience that distortion of results due to finite basin size is hard to avoid. This is because the radiation condition in the far field is difficult to fulfil for long waves. Reflection from distant boundaries such as the basin walls and wavemaker can introduce spurious peaks not present along an open coast, as pointed out theoretically by Santos & Peregrine (1998). Therefore for future planning of harbours and other coastal installations, stochastic theories aided by efficient computer algorithms and empirical corrections for various types of boundary dissipation may be a more reliable tool.

In principle the present method can be applied or extended to study slow-drift motions of moored ships or tethered offshore platforms in shallow seas. These problems are of increasing importance in the design of LNG (liquified natural gas) teminals. Near the scatterers, three-dimensional computations are needed, and must be matched with the mild-slope theory away from the scatterers.

The authors thank the US–Office of Naval Research (Grant N00014-04-1-0077), US National Science Foundation (Grant CTS-0075713) and US–Israel Binational Science Foundation for their financial support of this study.

REFERENCES

Bowers, E. C. 1977 Harbour resonance due to set-down beneath wave groups. *J. Fluid Mech.* **79**, 71–92.

Chamberlain, P. G. & Porter, D. 1995 The modified mild-slope equation. *J. Fluid Mech.* **291**, 393–407.

Chen, H. S. & Mei, C. C. 1974 Oscillations and wave forces in an offshore harbour. *Tech. Rep.* 190. Parsons Lab. Dept. Civil and Environm. Engng, MIT.

Chen, M.-Y. & Mei, C. C. 2006. Second-order refraction and diffraction of surface water waves. *J. Fluid Mech.* **552**, 137–166.

Hwang, L. S. & Tuck, E. O. 1970 On the oscillation of harbours of arbitrary shape. *J. Fluid Mech.* **42**, 447–464.

Kiatigorodskii, S. A., Krasitskii, V. P. & Zaslavskii, M. M. 1975 On Phillips' theory of equilibrium range in the spectra of wind-generated gravity waves. *J. Phys. Oceanogr.* **5**, 410–420.

Komen, G. J., Cavaleri, L., Donelan, M., Hasselmann, K., Hasselmann, S. & Janssen, P. A. E. M. 1994 *Dynamics and Modelling of Ocean Waves*. Cambridge University Press.

Lee, J. J. & Raichlen, F. 1972 Oscillations in harbour with connection basins. *J. Waterways, Harbours Coastal Engng Div. ASCE* **98**, 311–332.

Mei, C. C. 1983 *The Applied Dynamics of Ocean Surface Waves*. Word Scientific.

Mei, C. C. & Agnon, Y. 1989 Long-period oscillations in a harbour induced by incident short waves. *J. Fluid Mech.* **208**, 595–608.

Mei, C. C., Stiassnie, M. & Yue, D. K.-P. 2005 *Theory and Applications of Ocean Surface Waves, Part I*. World Scientific.

Miles, J. W. & Munk, W. 1961 Harbour paradox. *J. Waterways Harbour Div. ASCE* **87**, 111–130.

Ochi, M. 1998 *Ocean Waves, the Stochastic Approach*. Cambridge University Press.

Santos, J. A. & Peregrine, D. H. 1998 Trapped and free-wave propagation in channels and harbours. *Intl Conf. Coastal Engng*, ASCE Copenhagen, vol. **1**, pp. 244–257.

Sclavounos, P. D. 1992 On the quadratic effect of random gravity waves on a vertical boundary. *J. Fluid Mech.* **242**, 475–489.

Wu, J.-K. & Liu, P. L.-F. 1990 Harbour excitations by incident wave groups. *J. Fluid Mech.* **217**, 595–613.